The Astrophysical Journal, 779:120 (8pp), 2013 December 20 doi:10.1088/0004-637X/779/2/120

INDIRECT ULTRAVIOLET PHOTODESORPTION FROM CO:N_2 BINARY ICES — AN EFFICIENT GRAIN-GAS PROCESS

Mathieu Bertin[1], Edith C. Fayolle[2], Claire Romanzin[3], Hugo A. M. Poderoso[1], Xavier Michaut[1], Laurent Philippe[1], Pascal Jeseck[1], Karin I. Öberg[4], Harold Linnartz[2], and Jean-Hugues Fillion[1]
[1] Laboratoire de Physique Moléculaire pour l'Atmosphère et l'Astrophysique (LPMAA), CNRS UMR 7092, UPMC Univ. Paris 6, F-75252 Paris, France
[2] Sackler Laboratory for Astrophysics, Leiden Observatory, Leiden University, P.O. Box 9513, NL-2300-RA Leiden, The Netherlands
[3] Laboratoire de Chimie Physique (LCP), CNRS UMR 8000, Univ. Paris Sud 11, F-91400 Orsay, France
[4] Harvard-Smithsonian Center for Astrophysics, 60 Garden Street, Cambridge, MA 02138, USA
Received 2013 July 1; accepted 2013 October 14; published 2013 December 2

ABSTRACT

Ultraviolet (UV) ice photodesorption is an important non-thermal desorption pathway in many interstellar environments that has been invoked to explain observations of cold molecules in disks, clouds, and cloud cores. Systematic laboratory studies of the photodesorption rates, between 7 and 14 eV, from CO:N_2 binary ices, have been performed at the DESIRS vacuum UV beamline of the synchrotron facility SOLEIL. The photodesorption spectral analysis demonstrates that the photodesorption process is indirect, i.e., the desorption is induced by a photon absorption in sub-surface molecular layers, while only surface molecules are actually desorbing. The photodesorption spectra of CO and N_2 in binary ices therefore depend on the absorption spectra of the dominant species in the sub-surface ice layer, which implies that the photodesorption efficiency and energy dependence are dramatically different for mixed and layered ices compared with pure ices. In particular, a thin (1–2 ML) N_2 ice layer on top of CO will effectively quench CO photodesorption, while enhancing N_2 photodesorption by a factor of a few (compared with the pure ices) when the ice is exposed to a typical dark cloud UV field, which may help to explain the different distributions of CO and N_2H^+ in molecular cloud cores. This indirect photodesorption mechanism may also explain observations of small amounts of complex organics in cold interstellar environments.

Key words: astrochemistry – ISM: abundances – ISM: molecules – molecular processes

Online-only material: color figures

1. INTRODUCTION

In cold and dense regions of the interstellar medium (ISM), characteristic of star and planet formation, gaseous atoms, and molecules stick onto dust grains and form ice mantles in relatively short timescales. At these very low temperatures (<20 K), thermal desorption is negligible for all molecules except H_2. Yet, molecules are detected in the gas phase for temperatures below their condensation temperature and this implies the existence of efficient non-thermal desorption processes. These comprise desorption induced by cosmic rays, chemically induced desorption, and vacuum ultraviolet (VUV) photodesorption. The latter has been proposed as an important desorption pathway, particularly in the surface layers of protoplanetary disks (Dominik et al. 2005; Hogerheijde et al. 2011; Willacy & Langer 2000). It may also account for the gas-to-ice abundance ratio for a number of species as observed in other dense regions of the ISM (Coutens et al. 2012; Hollenbach et al. 2009), including the edges of molecular clouds where external UV photons can alter the ice mantle formation or in the inner part of dense molecular clouds where UV photons are produced by the cosmic-ray ionization of H_2 (Caselli et al. 2012). Photodesorption, therefore, is of general importance, influencing the chemistry at different locations in denser regions in space.

Quantitative photodesorption yields from low-temperature ices were first obtained experimentally for H_2O (Westley et al. 1995a, 1995b). Over the last 5–7 yr, photodesorption rates have been determined for other pure ice samples using broadband hydrogen discharge lamps: CO (Muñoz Caro et al. 2010; Oberg et al. 2007), H_2O/D_2O (Oberg et al. 2009b), N_2 and CO_2 (Bahr & Baragiola 2012; Oberg et al. 2009c; Yuan & Yates 2013), and O_2 and O_3 (Zhen & Linnartz 2013). Molecular dynamics calculations have been performed for water ice (Andersson et al. 2005, 2006; Arasa et al. 2011) and are in good agreement with the experimental findings. More recently, wavelength-specific studies have been performed and absolute photodesorption rates for CO, N_2, and O_2 have been determined between 7 and 14 eV (Fayolle et al. 2011, 2013). The spectral dependence of the photodesorption yield is of fundamental interest for modeling regions in space with different spectral energy distributions. Moreover, this approach has been very successful in linking the photodesorption process in the ice to the solid-state mechanisms at play, highlighting the physical–chemical parameters governing the photodesorption process. In the case of CO and N_2, the wavelength-dependent intensity of the measured photon-stimulated desorption (PSD) signals follows directly the electronic transitions in the condensed molecules (Fayolle et al. 2011, 2013). This is a signature of a mechanism known as Desorption Induced by Electronic Transition (DIET), not (substantially) involving dissociation/recombination in the ices. An even more detailed picture of the involved surface processes has been derived from the investigation of layered $^{13}CO/^{12}CO$ films (Bertin et al. 2012) showing that the photodesorption is mediated by the ice lattice. This study pointed out a sub-surface excitation mechanism in which electronically excited molecules release their energy through intermolecular vibrational motion into a desorption channel. Recently, Yuan & Yates (2013) addressed the crucial role of this energy transfer from the ice lattice by comparing Lyman α photodesorption at 75 K for pure $^{12}CO_2$, pure $^{13}CO_2$, and $^{12/13}CO_2$ mixed ices.

In the present work, we go one step further and study the photodesorption efficiency of a binary ice mixture made of different

chemical species. We present wavelength-dependent photodesorption measurements from CO and N_2 binary ices (layered and mixed) at 10 K. This is interesting from a physical–chemical point of view; their masses are nearly equivalent, their photodesorption mechanisms are similar, and their binding energies to the solid are comparable, but the two molecules have strong, non-coinciding photodesorption features in the VUV (around 8.5 and above 12.3 eV for CO and N_2, respectively) in their pure solid phase. The choice for a CO:N_2 ice is particularly relevant from an astronomical point of view. CO is highly abundant, both in the gas phase and in the solid state, representing the main molecular component after H_2. Molecular nitrogen, N_2, is not directly detectable due to its lack of a permanent dipole moment, but is considered to be one of the main reservoirs of nitrogen in the gas phase, due to its high stability. Its presence in the ISM is evidenced by the detection of N_2H^+ resulting from a proton transfer reaction involving H_3^+ (Bergin et al. 2002; Flower et al. 2006; Hily-Blant et al. 2010). Moreover, N_2 stands at the origin of other processes leading to the formation of more complex N-bearing molecules (Hily-Blant et al. 2013; Persson et al. 2010, 2012). As both CO and N_2 are highly volatile, with accretion temperatures in the 16–20 K regime under ISM conditions and sticking coefficients close to unity, they are the last species to freeze onto dust grains, generating a top layer that can be considered to be a binary interstellar ice (Bisschop et al. 2006; Oberg et al. 2005).

In this paper, we present a laboratory based study of VUV-irradiated CO:N_2 binary ice samples as a function of wavelength. This approach follows successful experiments of pure CO, N_2, and O_2 ices (Fayolle et al. 2011, 2013; Bertin et al. 2012). In the next section, experimental details are given. The results are presented in Section 3 and are discussed from a physical–chemical and an astrophysical point of view in Section 4.

2. EXPERIMENTAL METHODS

The photodesorption studies are realized in the Surface Processes and ICES (SPICES) setup of the Université Pierre et Marie Curie (UPMC), under ultra-high vacuum (UHV) conditions ($P \sim 1 \times 10^{-10}$ torr). The substrate on which ices are grown is a highly oriented polycrystalline graphite (HOPG) surface. It is mounted on the tip of a turnable cold head that can be cooled down to ∼10 K by means of a closed cycle helium cryostat. The ice layers are grown in situ by exposing the cold HOPG substrate to a partial pressure of CO and/or N_2 gases. A dosing tube, placed 1 mm in front of the substrate, allows a local exposure of the gases onto the cold sample without contaminating the whole UHV chamber. The isotopologues ^{13}CO (Eurisotop, 99.6% ^{13}C) and $^{15}N_2$ (Eurisotop, 97% ^{15}N) are used in order for them to be distinguishable by mass spectrometry. The quantities of molecules deposited on the substrate are expressed in monolayer equivalent (ML_{eq}) corresponding to the surface density of a compact molecular layer on a flat surface, with 1 $ML_{eq} \approx 1 \times 10^{15}$ molecule cm^{-2}. Temperature programmed desorption is used for the calibration of the ice thicknesses, resulting in reproducible parameters for the growth conditions with a precision better than 1 ML_{eq}.

UV photodesorption is induced through irradiation of the ice sample by the continuous output of the undulator-based VUV DESIRS beamline of the synchrotron SOLEIL (Nahon et al. 2012), providing photons with an energy that can be continuously scanned over the 7–14 eV range. A narrow bandwidth of typically 40 meV is selected by the 6.65 m normal incidence monochromator that is implemented on the beamline. A gas filter in the beamline suppresses the harmonics of the undulator that can be transmitted in higher diffraction orders of the grating. The absolute incident photon flux per surface unit impinging onto the sample is measured by a calibrated photodiode and varies for a given spectral bandwidth of 40 meV between 0.3 and 1.1×10^{13} photons s^{-1} cm^{-2}, depending on the photon energy. In order to prevent radiation cut-off, the DESIRS beamline is directly connected to SPICES, i.e., without any window.

The PSD spectra were obtained as follows. The signals of desorbing species with given masses are recorded as a function of time using a quadrupole mass spectrometer (QMS), while the sample is irradiated with photons whose energy is continuously scanned from 7 to 14 eV with steps of 25 meV. This gives the mass signal of desorbing species as a function of the incident photon energy, which can be converted into an absolute photodesorption yield in desorbed molecule per incident photon, using (1), the measured energy-dependent photon flux, and (2), the calibration of the mass signal into an absolute amount of desorbed molecules. More details on this calibration step have been previously given in Fayolle et al. (2011, 2013). It is important to note that this treatment does not significantly change the global shape of the PSD spectra: the observed structures in calibrated PSD spectra are already clearly visible in the unprocessed signals.

Each energy step lasts ∼5 s. In parallel, the QMS signal is recorded with a dwell of 1 s, which makes an average of five points per energy step. Caution has been taken to ensure that for each data point the 1 s accumulation time is substantially longer than the QMS mass signal build-up time, preventing eventual artifacts due to fast wavelength scanning. Each PSD spectrum from 7 to 14 eV is made continuously on the same sample. An energy scan from 7 to 14 eV lasts 23 minutes. From our calibrated PSD spectra and the evolution of the photon flux with time and energy, we can estimate the total amount of desorbed molecules per scan for each PSD spectrum. At the maximum, we find a total density of photodesorbed molecules of $\sim 10^{13}$ molecule cm^{-2}, which corresponds to 10^{-2} ML_{eq}. Therefore, the amount of photodesorbed molecules during one single scan is negligible compared with the total amount of molecules available in the ice, which at its lowest value amounts to 0.9 ML_{eq}. The photoprocessing of the ice is not expected to modify the photodesorption rate from the beginning to the end of the scan. This is confirmed experimentally since PSD spectra obtained two times in a row on the same sample are identical.

In order to make a clear separation between signals associated with ^{13}CO ($m = 29$ amu) and $^{15}N_2$ ($m = 30$ amu), we verified that our QMS mass resolution is sufficient to differentiate each mass peak. From the mass spectra of the pure products and the mixture of both, we derive a resolution of ∼0.3 amu, as taken from the full width at half maximum of the Gaussian mass peaks. It is accurate enough to allow for a fine separation of ^{13}CO and $^{15}N_2$ signals that have indeed a negligible overlap, as can be clearly seen in the corresponding mass spectra, available in Appendix.

3. RESULTS

Figure 1(a) shows PSD spectra obtained upon VUV irradiation of the pure ^{13}CO and $^{15}N_2$ ices. These spectra have already been presented and discussed in previous studies. The photodesorption rates exhibit energy-dependent efficiencies

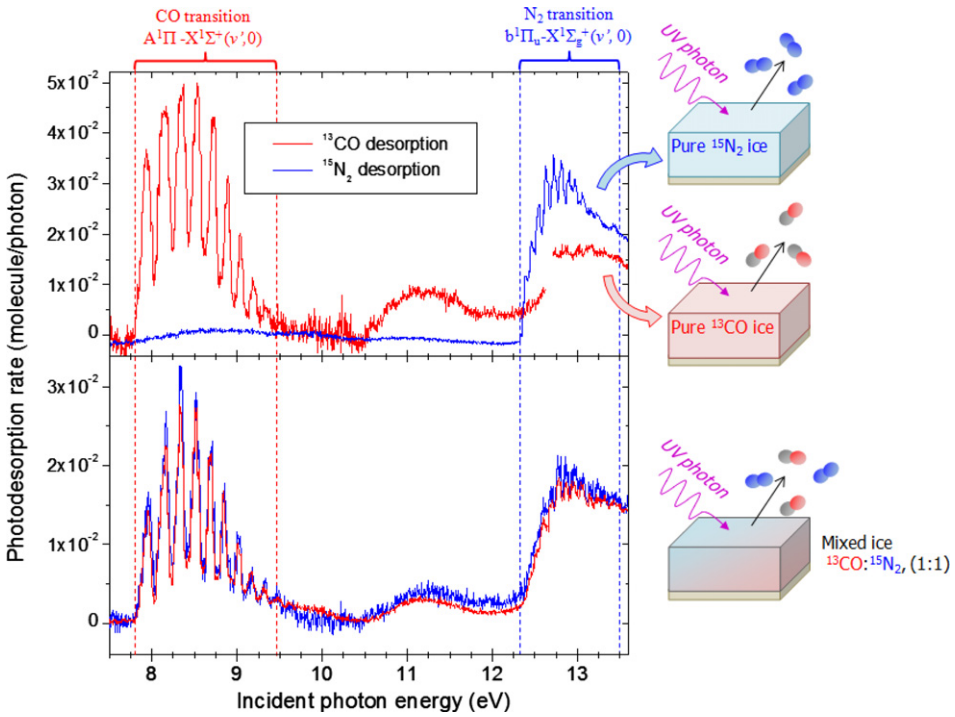

Figure 1. PSD spectra of ^{13}CO (red) and $^{15}N_2$ (blue) from 30 ML_{eq} of pure ^{13}CO and $^{15}N_2$ ices (a) and from a mixed ^{13}CO:$^{15}N_2$ ice, in a 1:1 proportion (b). The electronic transitions in condensed CO and N_2 associated with the main photodesorption features are indicated. All spectra have been obtained for ices kept at 15 K and deposited on HOPG.

(A color version of this figure is available in the online journal.)

that follow closely the VUV absorption of the pure molecular solids, with patterns that are associated with electronic transitions of the condensed molecules. For instance, the features observed between 7.9 and 9.5 eV in the CO PSD spectrum are due to vibronic bands in the $A^1\Pi$–$X^1\Sigma^+(v', 0)$ electronic transition, each peak being associated with a transition toward a vibrational sub-level v' in the A-state of solid ^{13}CO (Fayolle et al. 2011). In a similar way, the main feature responsible for the photodesorption of solid $^{15}N_2$ (above 12.3 eV) is associated with the $b^1\Pi_u$–$X^1\Sigma_g^+(v', 0)$ transition in pure nitrogen ice (Fayolle et al. 2013). The observation of such structures in the energy-resolved photodesorption rates is a clear signature for a DIET mechanism, as discussed in Fayolle et al. (2011, 2013). It has been shown that the excitation mainly takes place in a sub-surface region of the ice (two to three upper molecular layers), while only the molecules from the topmost layer are ejected into the gas phase. A short-range energy transfer from the excited to the desorbing molecules is therefore expected to occur, presumably through the coupling between the relaxation of the excited species and the excitation of intermolecular collective vibrational modes (Bertin et al. 2012). It should be noted that the thickness of our samples is less than the photon penetration depth, implying that photons can excite molecules deeper within the ice and even reach the graphite substrate. However, according to Bertin et al. (2012), neither the substrate nor underlying layers are contributing to the desorption features observed here. The question that is addressed here is how these properties translate in a mixed ice, consisting of both CO and N_2.

3.1. Photodesorption from Mixed CO:N_2 Ice

Figure 1(b) shows the PSD spectra for both ^{13}CO and $^{15}N_2$ desorbing upon VUV irradiation of an ice grown from a 1:1 CO:N_2 mixture. There is a clear difference between the results for the pure and mixed ice irradiation. As discussed above, the pure ice spectra are very different, whereas, for the mixed ice, the PSD spectra are identical. A comparison with Figure 1(a) shows that the photodesorption spectra of the CO:N_2 ice mixture results in a superposition of the PSD spectra of the two pure constituents. The ejection of any surface molecule in the mixed ice is clearly initiated by the electronic excitation of any other molecule. In particular, the PSD spectra of the mixed ice show that the excitation of solid CO into its $A^1\Pi$ state leads to the desorption of surface N_2 (7.9–9.5 eV) and that solid N_2 excitation into its $b^1\Pi_u$ state initiates CO desorption above 12.3 eV. This finding is fully consistent with the previously introduced concept of an indirect DIET mechanism; part of the excess energy deposited in the ice by the VUV photon absorption is transferred from one to the other molecule independently of its chemical nature—causing desorption.

For a given energy, the absolute photodesorption rates of CO and N_2 from the mixed ice are lower by a factor of two than the corresponding value derived for the pure ices. In fact, the PSD spectra of the mixture can be fitted with very good agreement by a linear combination of the desorption spectra of pure $^{15}N_2$ and pure ^{13}CO, in which each constituent contributes to about ∼0.5 of the overall desorption signal (Figure 2). As the surface of the mixed film is expected to be composed of half CO and half N_2 molecules and as the adsorption energies of CO and N_2 are very close (Bisschop et al. 2006), this shows that the amount and efficiency of the energy transfer to surface molecules upon sub-surface CO excitation or N_2 excitation are about the same.

3.2. Photodesorption from Layered N_2/CO and CO/N_2 Ices

PSD spectra of ^{13}CO (left panel) and $^{15}N_2$ (right panel) obtained from a pure 25 ML_{eq} ^{13}CO ice covered by an increasing layer of $^{15}N_2$ are shown in Figure 3. In the case of pure CO or N_2

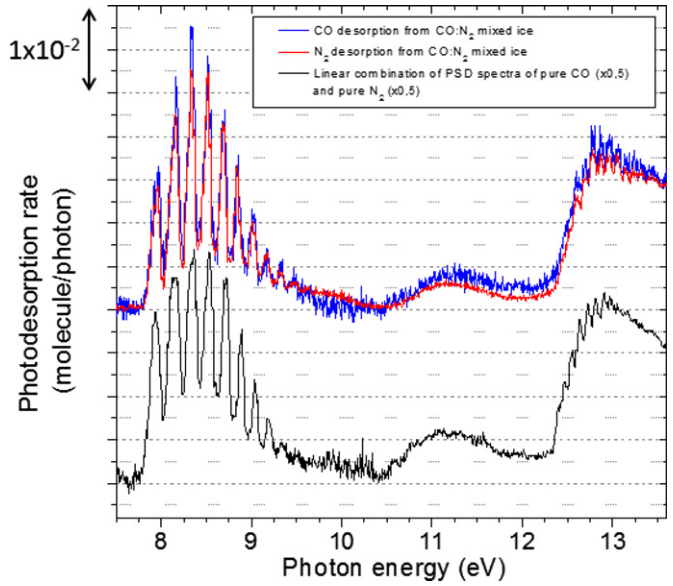

Figure 2. Photon-stimulated spectra of $^{15}N_2$ and ^{13}CO from a mixed ^{13}CO:$^{15}N_2$ 30 ML_{eq} ice, in a 1:1 proportion, compared with a linear combination of PSD spectra obtained from pure ^{13}CO ice (×0.5) and pure $^{15}N_2$ ice (×0.5). The spectra have been acquired from ices deposited on HOPG kept at 15 K.

(A color version of this figure is available in the online journal.)

ice (top left and bottom right, respectively), the characteristic desorption profiles around 8.5 and above 12.3 eV are seen. When the CO ice is covered by 0.9 ML_{eq} of N_2, the CO desorption yield drops substantially and it is almost entirely suppressed above ML_{eq}. This behavior, also observed in the case of layered $^{13}CO/^{12}CO$ (Bertin et al. 2012), shows that mostly the surface molecules are susceptible to desorb upon UV irradiation.

When investigating the PSD of $^{15}N_2$ for a low thickness of N_2 overlayer (0.9 ML_{eq}), one can see that its photodesorption pattern mimics almost completely the one of the pure CO ice, demonstrating that its photodesorption is triggered only by the absorption of the underlying CO molecules. In particular, its photodesorption in the 7.9–9.5 eV range, associated with the excitation of the $A^1\Pi$ state of solid CO, becomes the dominant contribution, although pure solid N_2 does not photodesorb at these energies. In contrast, photodesorption initiated by the N_2 excitation in the $b^1\Pi_u$ state (>12.3 eV) is not clearly observed. This cannot be explained by the lack of surface N_2 at the end of the energy scan, since less than 0.01 ML_{eq} of N_2 has been ejected into the gas phase during the acquisition time. The adsorption of a small quantity of N_2 onto a CO ice therefore drastically modifies the energy dependence of its photodesorption process. For increasing thickness of the $^{15}N_2$ overlayer, the N_2 excitation contribution to the N_2 PSD spectra gradually approaches that of the pure N_2 ice. The contribution of the CO excitation becomes very weak for N_2 thicknesses above 2.5 ML_{eq}, showing that the range for an efficient energy transfer involves fewer than three molecular layers.

Figure 4 shows the results of layered experiments in which 25 ML_{eq} $^{15}N_2$ ice is covered by an increasing layer of ^{13}CO. The experiment is essentially identical to the previous one (Figure 3), but the role of N_2 and CO are exchanged. The N_2 photodesorption signal vanishes for a larger CO coverage and a clear vibrational progression in the ^{13}CO desorption channel is found that corresponds to an excitation into the $b^1\Pi_u$ state of N_2. This feature is superimposed over a continuous desorption of ^{13}CO observed above 12.5 eV in pure CO samples (Fayolle et al. 2011). As for the 25 ML_{eq} ^{13}CO ice covered by $^{15}N_2$, the spectra are fully consistent with a process in which only surface molecules desorb after excitation of sub-surface species.

4. DISCUSSIONS AND ASTROPHYSICAL IMPLICATIONS

4.1. The Role of Ice Structure and Composition on Absolute Photodesorption Rates

The VUV photodesorption of coadsorbed N_2 and CO presents very different energy-dependent profiles and efficiencies compared with pure N_2 and CO ices. Both molecules mainly

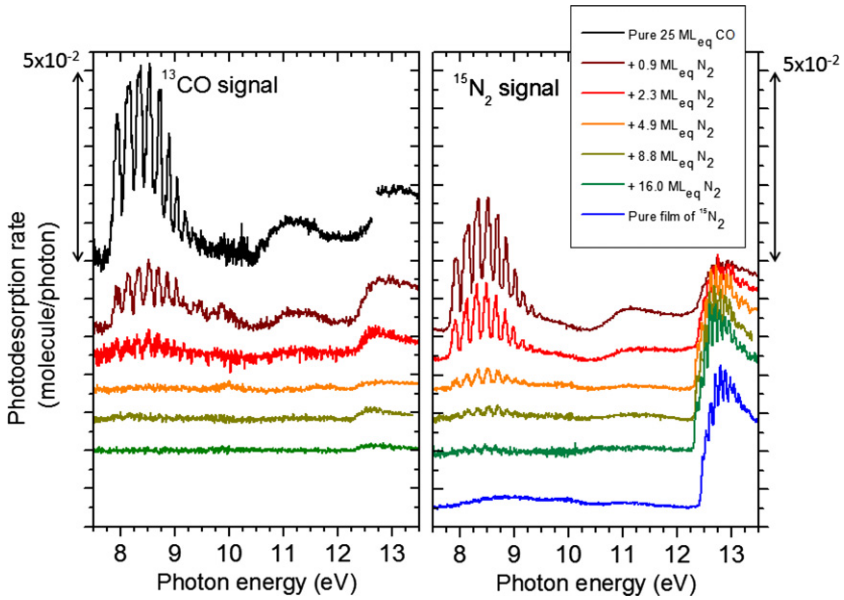

Figure 3. PSD spectra of ^{13}CO (left) and $^{15}N_2$ (right) from 25 ML_{eq} of ^{13}CO ice covered by an increasing $^{15}N_2$ layer on top. The PSD spectrum obtained from a pure 25 ML_{eq} $^{15}N_2$ ice is also presented for comparison. All spectra are recorded for 15 K ices, deposited on HOPG.

(A color version of this figure is available in the online journal.)

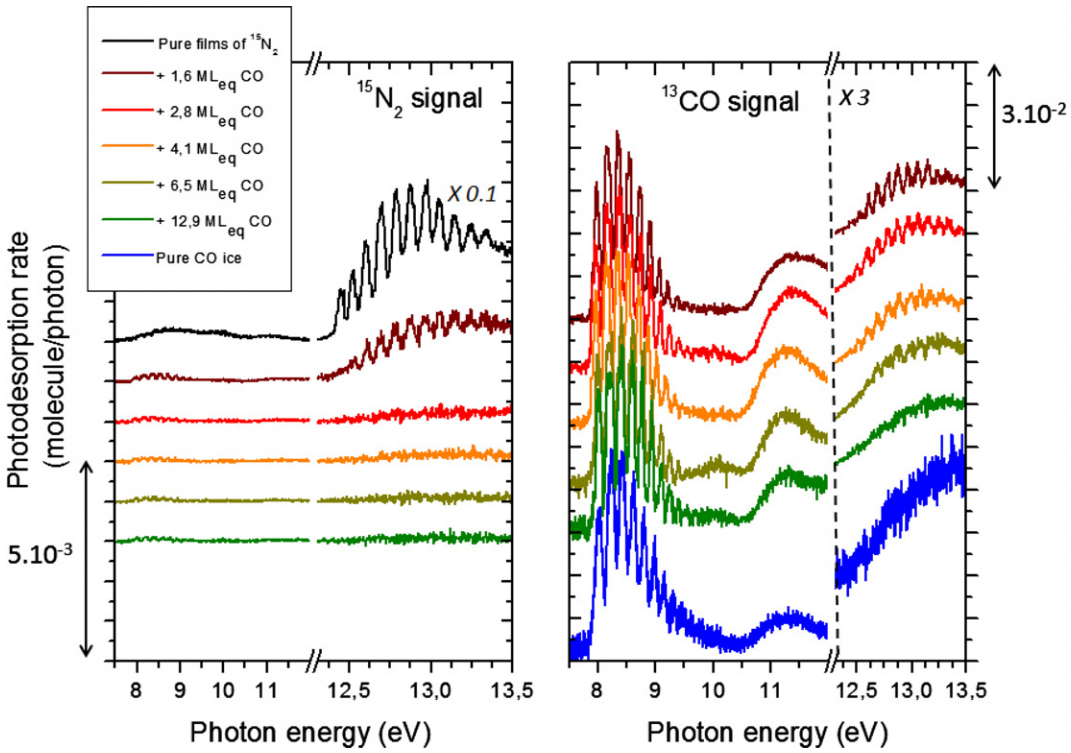

Figure 4. PSD spectra of $^{15}N_2$ (left) and ^{13}CO (right) from 25 ML_{eq} of $^{15}N_2$ ice covered by an increasing layer of ^{13}CO ice on top. All spectra are recorded for 15 K ices, deposited on HOPG. The top spectra in the left panel (photodesorption of N_2 from a pure N_2 ice) have been multiplied by 0.1 for visual clarity. In the right panel, the CO PSD spectra in the 12.3–13.5 eV energy range have been multiplied by 3.

(A color version of this figure is available in the online journal.)

desorb through an indirect mechanism, where the excitation of a sub-surface molecule, whether CO or N_2, leads to the desorption of N_2 and CO surface molecules. Because this indirect mechanism involves energy transfer from the excited molecule to the desorbing one, presumably by collective vibrational mode excitation, the photodesorption energy dependence and efficiency depend strongly on the nature of the intermolecular interactions. In general, intermolecular interactions in solids may promote the photodesorption, but also quench it. This has been demonstrated for CO_2 in interaction with other isotopologues or rare gas matrices (Yuan & Yates 2013) and for CO in interaction with H_2O ice (Bertin et al. 2012). For the latter case, an explanation has been proposed, stating that the photodesorption efficiency is driven by the competition between two excess energy relaxation pathways: (1) relaxation by intermolecular phonon modes of the ice, coupled with desorption and (2) relaxation by transfer to intramolecular vibration modes of neighboring molecules. If the first relaxation pathway is dominant, the photodesorption will be efficiently triggered by UV absorption of the neighboring molecule. If the latter pathway dominates, the relaxation process, as is the case when excited CO transfers efficiently its excess energy to the O–H dangling bond vibrations of neighboring water molecules, then the photodesorption is hindered. In both cases, the constructive and destructive matrix effects are a consequence of the indirect character of the photodesorption mechanism.

Because the intermolecular coupling in the ice between excited and surface molecules can drastically modify the photodesorption process, it is expected that different compositions, but also different structures of the ice, will modify the energy-integrated photodesorption yield for a given UV field. This is illustrated for the N_2/CO binary ices. As shown in Figures 1 and 3, coadsorption of N_2 with CO promotes N_2 desorption in the 7–11.5 eV range whereas it decreases the desorption efficiency of CO in the same energy range. To quantify this effect, energy-integrated photodesorption rates have been derived from our PSD curves for three types of interstellar VUV profiles as a function of the CO:N_2 layered/mixed ices composition. The results are displayed in Table 1. To obtain these values, our energy-resolved desorption rates have been convoluted with VUV profiles describing the interstellar radiation field at the edge of clouds (Mathis et al. 1983), the effect of secondary photons from cosmic-ray impacts in dense cores (Gredel et al. 1987), and a TW Hydræ radiation field as model for the UV field in protoplanetary disks (Herczeg et al. 2002; Valenti et al. 2003; Johns-Krull & Herczeg 2007). The resulting photodesorption rates vary depending on (1) the UV field considered, (2) the ice composition, and (3) the internal ice organization (layered versus mixed). Compared with pure ices, the photodesorption rates from the binary ices change by up to an order of magnitude. The general trend is to decrease the CO photodesorption rate from $>1 \times 10^{-2}$ to 2–6 $\times 10^{-3}$ molecules photon^{-1} and to increase the N_2 photodesorption rate by a factor of 2–3. This shows that a proper description of the VUV photodesorption process has to take into consideration the structure and composition of the ice on which the molecules are adsorbed; the photodesorption rates extracted from pure molecular solids may not be realistic in the case of more complex ices, as typically present in the ISM.

4.2. Implications for N_2 and CO Gas-phase Abundance in Dense Cores

In dense cores, N_2 and CO are expected to freeze out onto dust grains at very low temperatures, less than 2 K apart,

Table 1
Energy-integrated Photodesorption Rates of CO and N_2 in Several Regions of the ISM for Pure Ices, Mixed CO:N_2 Ices in a 1:1 Proportion, and a 0.9 Monolayer Equivalent (ML_{eq}) of N_2 Deposited on Top of a CO Ice

Environment	Pure	Pure	CO from		N_2 from	
	CO ice[d]	N_2 ice[e]	Mixture CO:N_2 1:1	0.9 ML_{eq} N_2 on CO	Mixture CO:N_2 1:1	0.9 ML_{eq} N_2 on CO
Edges of clouds[a]	1.3×10^{-2}	2.6×10^{-3}	5.7×10^{-3}	5.3×10^{-3}	5.5×10^{-3}	8.0×10^{-3}
Prestellar cores[b]	1.0×10^{-2}	2.2×10^{-3}	3.0×10^{-3}	3.9×10^{-3}	3.0×10^{-3}	5.1×10^{-3}
Protoplanetary disk[c]	7.2×10^{-2}	5.3×10^{-3}	2.3×10^{-3}	3.0×10^{-3}	2.1×10^{-3}	2.7×10^{-3}

Notes. The rates are for ices kept at 15 K. All values are given in desorbed molecules per incident photon. Using the UV field from [a]Mathis et al. 1983, [b]Gredel et al. 1987, [c]Herczeg et al. 2002, Valenti et al. 2003, Johns-Skrull & Herczeg 2007. [d] and [e] are values from Fayolle et al. 2011 and Fayolle et al. 2013, respectively.

and with the same sticking efficiency (Bisschop et al. 2006; Oberg et al. 2007). Consequently, a similar depletion in the gas phase should be observed. Nevertheless, observational studies of N_2H^+ and other N-containing species in dense cores providing data to indirectly derive the N_2 abundance suggest that N_2 depletion on grains occurs later, i.e., at a higher density, than for CO (Bergin et al. 2002; Pagani et al. 2005, 2012). Therefore, it has been suggested that another mechanism is responsible for a continuous enrichment of gas-phase N_2, counterbalancing its accretion onto grains. Chemistry involving CN + N reactions, constantly forming N_2 in the gas, is invoked (Hily-Blant et al. 2010). Non-thermal desorption processes, such as photodesorption, could also contribute to this effect by preferentially ejecting N_2 instead of CO in the gas phase. Nevertheless, the photodesorption rates as extracted from pure CO and N_2 ices cannot resolve this issue since for realistic dark cloud UV fields the photodesorption rate is substantially lower for pure N_2 than for pure CO ice (Table 1). However, considering pure ices only may be inappropriate, as discussed in Section 4.1, since ice structure and composition influence the CO and N_2 photodesorption rates.

Since CO and N_2 are expected to freeze out in the same temperature range, it is rather unlikely that the top layers of the ices are composed solely of pure N_2 or pure CO thick layers. Instead, we expect that both species are coadsorbed at the surface of the icy grains. The exact nature of the top layers depends on the total abundance of N_2 as compared with CO, as well as on the proximity in time and space of CO and N_2 freeze out. As the amount of gas-phase N_2 is relatively low compared with CO (Bergin et al. 2002; Maret et al. 2006), it is expected that solid-phase N_2 will be embedded in a CO-rich environment. Whether the outer layers of the grain will be layered or mixed is not easy to answer and is likely source-dependent. N_2 is expected to condense for a temperature that is 2 K lower than for CO (Flower et al. 2006; Hily-Blant et al. 2010), which would, for low cooling speed of the cloud, lead to the growth of a thin N_2 layer on top of CO-rich ice. In the case of a shorter cooling time, such a temperature difference would not be sufficient to result in segregated layers and N_2 would be intimately mixed with the CO.

Table 1 shows that for realistic dark cloud UV fields photodesorption rates extracted from pure N_2 ice are substantially lower for than for pure CO ice. If we consider instead mixed CO:N_2 1:1 ice, the photodesorption rates of CO and N_2 in prestellar cores are identical. In the case of a more realistic system, i.e., a small amount (0.9 ML_{eq}) of N_2 on CO ice, then the CO photodesorption rate strongly decreases, whereas the N_2 photodesorption rate increases. Then, the N_2 desorption becomes more efficient than the CO desorption and photodesorption can contribute to a gas-phase N_2 enrichment. We conclude that under interstellar conditions N_2 will be photodesorbed at least as efficiently as CO as long as they are coadsorbed. In many core environments, the N_2 photodesorption may exceed that of CO, providing a natural explanation as to why N_2 is maintained longer in the gas phase compared with CO.

4.3. Organics Desorption Through CO Photoexcitation?

The indirect nature of the photodesorption process may have general implications beyond the explanation of the CO and N_2 abundances in the ISM. The ability of CO ice to transfer part of the absorbed energy to a surrounding molecule may act as an important indirect photodesorption channel of other species as well. This could be true in particular for chemically linked formaldehyde H_2CO and methanol CH_3OH and possibly even more complex organic molecules, providing a non-dissociative, non-thermal desorption pathway. Indeed, such organics are expected to efficiently photodissociate upon UV photon irradiation, as it has been found for CH_3OH (Oberg et al. 2009a), leading to the formation of photoproducts that can eventually desorb. Embedded in a CO-rich environment, however, such molecules may react differently under UV irradiation: a photon absorption by the surrounding and more numerous CO molecules could lead to the desorption of the surface-located organics via a similar mechanism as highlighted for CO:N_2. Such a process could then explain the gas abundances of organics, observed in the cold regions of the ISM (Bacmann et al. 2012; Oberg et al. 2010; Tercero et al. 2013). Whether this indirect photodesorption process can be generalized to heavier and more strongly bound species than CO and N_2 needs to be experimentally verified, however.

5. SUMMARY AND CONCLUSIONS

From a systematic set of energy-resolved (7–14 eV; 40 meV) photodesorption laboratory studies on CO:N_2 binary ices, both mixed and layered, the following conclusions can be drawn.

1. The desorption is induced by a photon absorption in the topmost molecular layers, while only surface molecules are actually desorbing. This implies an energy transfer from the sub-surface excited molecule to the surface ones. Thus, the photodesorption rate is not linked to the absorption spectrum of the desorbing molecule, but is instead associated with the absorption profile of the surrounding species, located deeper in the ice. When N_2 and CO are mixed in equal proportions, their photodesorption spectra become

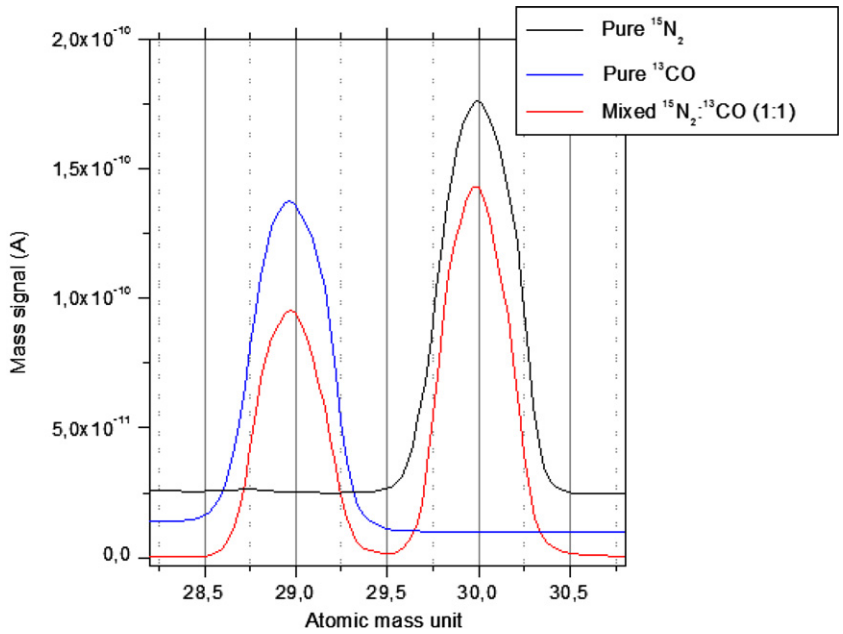

Figure 5. Mass spectra obtained from introduced partial pressure of (1) $\sim 10^{-9}$ torr of $^{15}N_2$, (2) $\sim 10^{-9}$ torr of ^{13}CO, and (3) a mixture of $\sim 10^{-9}$ torr of $^{15}N_2$ + $\sim 10^{-9}$ torr of ^{13}CO.

(A color version of this figure is available in the online journal.)

superimposable and reflect a linear combination of the photodesorption spectra of both pure ices. When a small quantity of N_2 is deposited at the surface of a CO ice, its photodesorption spectrum reflects mostly that of pure CO. This is remarkable since, in this case, the N_2 major desorption feature lies in the 7.9–9.5 eV energy range, in which pure solid N_2 does not absorb.

2. This indirect desorption mechanism and its dependence on ice structure and wavelength influence the (overall) desorption efficiency in space. Considering the range of indirect photodesorption processes, we suggest that the photodesorption rates experimentally obtained from pure ices should only be used for molecules that can form pure phases in the ISM ices, exceeding at least two to three molecular top layers, as it may be the case for CO in some cold regions (Pontoppidan et al. 2008, 2003). Below this thickness, or when molecules are mixed with others, photodesorption rates obtained from a more realistic composite ice should lead to a more accurate description of the non-thermal desorption. Here, both chemical composition and molecular organization play a role.
3. The results presented here provide a way to replenish nitrogen in prestellar cores, contributing to the unexplained low depletion rate of N_2 as compared with CO. If the rates derived for pure CO and N_2 are used, CO should desorb with an efficiency that is almost one order of magnitude higher than for N_2. This is not in agreement with observations that conclude that gaseous CO depletes on the grains with a higher rate than N_2 (Pagani et al. 2012). When considering the rates extracted from a more realistic system, most probably a layered N_2/CO structure with a small amount of N_2, as presented here, gaseous N_2 will be enriched with respect to CO. A detailed astrochemical modeling is required to quantify the extent of this N_2 enrichment.
4. Finally, the mechanism introduced here may act as a more general desorption process in other mixed ices of astrophysical interest. The CO present in CO-rich icy mantles has the potential to transfer photon energy to the kinetic energy of the surrounding molecules, triggering their photodesorption in an indirect way. The concerned species could be coadsorbed molecules during the freeze-out process, such as unsaturated carbon chains, but also small organics originating from the hydrogenation of CO, such as H_2CO and CH_3OH.

We acknowledge SOLEIL for providing of synchrotron radiation facilities under the project 20120834 and we thank Nelson De Oliveira for assistance on the beamline DESIRS. Financial support from the French CNRS national program Physique et Chimie du Milieu Interstellaire, the UPMC platform for astrophysics "ASTROLAB," the Dutch program Nederlandse Onderzoekschool voor Astronomie, and the Hubert Curien Partnership Van Gogh (25055YK) are gratefully acknowledged. The Leiden group acknowledges NWO support through a VICI grant.

APPENDIX

SEPARATION OF $^{15}N_2$ AND ^{13}CO SIGNALS BY MASS SPECTROMETRY

The study of the photodesorption of N_2 and CO from mixed ice requires a fine separation of the gas-phase signals associated with each molecule. In their most abundant isotopic form, $^{14}N_2$ and $^{12}C^{16}O$, both species have the same mass and cannot be separated by mass spectrometry. We therefore have used the isotopologues $^{13}C^{16}O$ and $^{15}N_2$ with respective masses of 29 amu and 30 amu. To ensure that the rise of one given mass signal does not lead to the artificial increase of the neighboring mass channel, it is necessary to check that the width of each mass signal is narrow enough to prevent significant overlap between the associated mass peaks. Figure 5 shows mass spectra, i.e., signals of the singly ionized gas-phase species as a function of its mass, realized when a pressure of (1) pure $^{15}N_2$, (2) pure ^{13}CO, and (3) mixed ^{13}CO:$^{15}N_2$ in a 1:1 proportion is introduced into the chamber. The mass peaks of $^{15}N_2$ ($m = 30$ amu) and

^{13}CO ($m = 29$ amu) are clearly separated. The rise of one mass signal does not lead to a measurable increase of the other mass channel. Moreover, the mass spectrum associated with the gaseous mixture exhibits no overlap between the two mass peaks. In the photodesorption experiments that are presented, the signals in the mass channel at 29 amu or 30 amu can therefore be associated unambiguously with the presence of ^{13}CO or $^{15}N_2$ gas, respectively.

REFERENCES

Andersson, S., Al-Halabi, A., Kroes, G. J., & van Dishoeck, E. F. 2006, JChPh, 124, 064715
Andersson, S., Kroes, G. J., & van Dishoeck, E. F. 2005, CPL, 408, 415
Arasa, C., Andersson, S., Cuppen, H. M., van Dishoeck, E. F., & Kroes, G. J. 2011, JChPh, 134, 9
Bacmann, A., Taquet, V., Faure, A., Kahane, C., & Ceccarelli, C. 2012, A&A, 541, L12
Bahr, D. A., & Baragiola, R. A. 2012, ApJ, 761, 36
Bergin, E. A., Alves, J., Huard, T., & Lada, C. J. 2002, ApJL, 570, L101
Bertin, M., Fayolle, E. C., Romanzin, C., et al. 2012, PCCP, 14, 9929
Bisschop, S. E., Fraser, H. J., Oberg, K. I., van Dishoeck, E. F., & Schlemmer, S. 2006, A&A, 449, 1297
Caselli, P., Keto, E., Bergin, E. A., et al. 2012, ApJL, 759, L37
Coutens, A., Vastel, C., Caux, E., et al. 2012, A&A, 539, 12
Dominik, C., Ceccarelli, C., Hollenbach, D., & Kaufman, M. 2005, ApJL, 635, L85
Fayolle, E. C., Bertin, M., Romanzin, C., et al. 2011, ApJL, 739, L36
Fayolle, E. C., Bertin, M., Romanzin, C., et al. 2013, A&A, 556, A122
Flower, D. R., Pineau des Forets, G., & Walmsley, C. M. 2006, A&A, 456, 215
Gredel, R., Lepp, S., & Dalgarno, A. 1987, ApJL, 323, L137
Herczeg, G. J., Linsky, J. L., Valenti, J. A., Johns-Krull, C. M., & Wood, B. E. 2002, ApJ, 572, 310
Hily-Blant, P., Bonal, L., Faure, A., & Quirico, E. 2013, Icar, 223, 582
Hily-Blant, P., Walmsley, M., Pineau des Forets, G., & Flower, D. 2010, A&A, 513, 20
Hogerheijde, M. R., Bergin, E. A., Brinch, C., et al. 2011, Sci, 334, 338
Hollenbach, D., Kaufman, M. J., Bergin, E. A., & Melnick, G. J. 2009, ApJ, 690, 1497
Johns-Krull, C. M., & Herczeg, G. J. 2007, ApJ, 655, 345
Maret, S., Bergin, E. A., & Lada, C. J. 2006, Natur, 442, 425
Mathis, J. S., Mezger, P. G., & Panagia, N. 1983, A&A, 128, 212
Muñoz Caro, G. M., Jimenez-Escotar, A., Martin-Gago, J. A., et al. 2010, A&A, 522, A108
Nahon, L., de Oliveira, N., Garcia, G. A., et al. 2012, J. Synchrotron Radiat., 19, 508
Oberg, K. I., Fuchs, G. W., Awad, Z., et al. 2007, ApJL, 662, L23
Oberg, K. I., Garrod, R. T., van Dishoeck, E. F., & Linnartz, H. 2009a, A&A, 504, 891
Oberg, K. I., Linnartz, H., Visser, R., & van Dishoeck, E. F. 2009b, ApJ, 693, 1209
Oberg, K. I., Qi, C., Fogel, J. K. J., et al. 2010, ApJ, 720, 480
Oberg, K. I., van Broekhuizen, F., Fraser, H. J., et al. 2005, ApJL, 621, L33
Oberg, K. I., van Dishoeck, E. F., & Linnartz, H. 2009c, A&A, 496, 281
Pagani, L., Bourgoin, A., & Lique, F. 2012, A&A, 548, L4
Pagani, L., Pardo, J. R., Apponi, A. J., Bacmann, A., & Cabrit, S. 2005, A&A, 429, 181
Persson, C. M., Black, J. H., Cernicharo, J., et al. 2010, A&A, 521, 6
Persson, C. M., Deluca, M., Mookerjed, B., et al. 2012, A&A, 543, 34
Pontoppidan, K. M., Boogert, A. C. A., Fraser, H. J., et al. 2008, ApJ, 678, 1005
Pontoppidan, K. M., Fraser, H. J., Dartois, E., et al. 2003, A&A, 408, 981
Tercero, B., Kleiner, I., Cernicharo, J., et al. 2013, ApJL, 770, L13
Valenti, J. A., Fallon, A. A., & Johns-Krull, C. M. 2003, Ap&SS, 147, 305
Westley, M. S., Baragiola, R. A., Johnson, R. E., & Baratta, G. A. 1995a, Natur, 373, 405
Westley, M. S., Baragiola, R. A., Johnson, R. E., & Baratta, G. A. 1995b, P&SS, 43, 1311
Willacy, K., & Langer, W. D. 2000, ApJ, 544, 903
Yuan, C. Q., & Yates, J. T. 2013, JChPh, 138, 154303
Zhen, J., & Linnartz, H. 2013, MNRAS, submitted